

Effect of color superconductivity on the mass of hybrid neutron stars in an effective model with perturbative QCD asymptotics

David Blaschke^{1,*}, Udit Shukla^{1,†}, Oleksii Ivanytskyi^{1,‡} and Simon Liebong^{2,§}

¹*Institute of Theoretical Physics, University of Wrocław, 50-204 Wrocław, Poland*

²*Institute for Theoretical Physics, TU Bergakademie Freiberg, 09599 Freiberg, Germany*



(Received 11 January 2023; accepted 7 March 2023; published 31 March 2023)

The effective cold quark matter model by Alford, Braby, Paris, and Reddy (ABPR) is used as a tool for discussing the effect of the size of the pairing gap in three-flavor (CFL) quark matter on the maximum mass of hybrid neutron stars (NSs). This equation of state (EOS) has three parameters which we suggest to determine by comparison with a nonlocal Nambu-Jona-Lasinio (nNJL) model of quark matter in the nonperturbative domain. We show that due to the momentum dependence of the pairing which is induced by the nonlocality of the interaction, the effective gap parameter in the EOS model is well approximated by a constant value depending on the diquark coupling strength in the Nambu-Jona-Lasinio (NJL) model Lagrangian. For the parameter $a_4 = 1 - 2\alpha_s/\pi$ a constant value below about 0.4 is needed to explain hybrid stars with $M_{\max} \gtrsim 2.0M_{\odot}$, which would translate to an effective constant $\alpha_s \sim 1$. The matching point with a running coupling at the 1-loop β function level is found to lie outside the range of chemical potentials accessible in NS interiors. A dictionary is provided for translating the free parameters of the nNJL model to those of the ABPR model. Both models are shown to be equivalent in the nonperturbative domain but the latter one allows to quantify the transition to the asymptotic behavior in accordance with perturbative QCD. We provide constraints on parameter sets that fulfill the $2M_{\odot}$ mass constraint for hybrid NSs, as well as the low tidal deformability constraint from GW170817 by a softening of the EOS on the hybrid NS branch with an early onset of deconfinement at $M_{\text{onset}} < 1.4M_{\odot}$. We find that the effective constant pairing gap should be around 100 MeV but not exceed values of about 130 MeV because a further increase of the gap would entail a softening of the EOS and contradict the $2M_{\odot}$ mass constraint.

DOI: 10.1103/PhysRevD.107.063034

I. INTRODUCTION

Two limits of the cold dense matter equation of state (EOS) are precisely known: (1) the state of nuclear matter at the nuclear saturation density $n_0 = 0.15 \text{ fm}^{-3}$ and below it; and (2) the cold quark matter EOS of perturbative QCD above about $40 n_0$. In between these limits the deconfinement phase transition has to take place. But the open question is whether its place could be in neutron star (NS) interiors.

By the end of the 1980s, the answer to this question by the authorities in the field was negative [1] were it not for the possibility of exotic strange stars [2–7], made up of absolutely stable strange quark matter (SSQM) [8]. At that time, works on stable quark matter cores in NSs like Ref. [9] not relying on the SSQM hypothesis but rather on assumptions for an interaction energy density functional were rather an exception. The nonrelativistic density

functional of the confining string-flip model (SFM) [10] that was used in [9] was recently generalized in a relativistic path integral formulation [11] which was successfully applied to study hybrid NSs, even forming a third family of compact stars [12,13].

Among the density functionals for describing dense quark matter, those of the Nambu-Jona-Lasinio (NJL) type with relativistic current-current interactions obeying chiral symmetry but lacking confinement [14,15] have been widely used, also in considering the question of quark matter deconfinement in NS interiors. These studies have shown that for a successful description of NS phenomenology with hybrid star sequences, two ingredients beyond the minimal NJL model interaction were essential: a vector meson channel for stiffening high-density quark matter, thus describing high-mass NSs and a scalar diquark interaction channel for lowering the onset of deconfinement [16,17]. For a recent review on the role of stiffness and color superconductivity in the description of the hadron-to-quark matter transition in NSs, see [18]. To remedy the lack of confinement that limits the application of NJL-type models to the $T = 0$ region of the QCD phase diagram, the confining density functional approach has recently been

*david.blaschke@uwr.edu.pl

†udita.shukla28@gmail.com

‡oleksii.ivanytskyi@uwr.edu.pl

§science@liebong.cc

developed to contain chiral symmetry and diquark interactions in the effective Lagrangian [19]. While this approach and its generalization to finite temperatures [20] was still concerned with two quark flavors only, a special simplified version for three massless quark flavors in the color flavor locking (CFL) phase with a very early deconfinement transition triggered by light sexaquark condensation has been developed in [21]. The corresponding CFL phase with three degenerate light quark flavors may be called CFL-light (CFLl). It is worth mentioning, that an early transition to such a three-flavor CFL phase rather than to the two-flavor color superconducting quark matter is in line with the argument of high energy cost caused by imposing electric and color neutrality in the two-flavor case [22]. At the same time, electric neutrality of the CFL phase is provided automatically and does not cause an increase of its free energy [23].

Coming back to the present work, namely to join the nuclear matter phase with asymptotic perturbative QCD matter, we face the problem that the most advanced density functional approaches to cold quark matter (NJL and SFM) do not possess the pQCD limit, which may conveniently be characterized by approaching the conformal limit for the squared speed of sound, $c_s^2 = 1/3$, from below. The persistence of collective mean fields in the vector and diquark sector even at asymptotic densities makes NJL and SFM models violate the conformal limit. Since central densities in NSs reach only about $5 n_0$, one might argue that it shall not be a problem at all to construct a matching with the pQCD EOS at $40 n_0$, which fulfills the basic constraints of causality ($c_s^2 \leq 1$) and thermodynamic stability. But as it has been shown in [24], there are EOS, e.g., in the ComPOSE library of compact star EOS [25] which do not allow such a matching unless it is introduced at sufficiently low densities and thus having an influence on the NS EOS.

Within the confining density functional approach, a procedure has been suggested that suggests a microscopic calculation of the medium dependence of vector and diquark coupling constants using a massive gluon propagator ansatz, so that the conformal limit is restored [26], see also [27].

In the present work, we want to suggest another approach to define a quark matter EOS that unifies the requirement of a pQCD asymptotics at high densities with the nonperturbative features of confinement and color superconductivity in the region of the hadron-to-quark matter transition that likely takes place in the interior of light NSs and is advantageous for fulfilling modern multi-messenger constraints of NS phenomenology. The effective quark matter EOS suggested by Alford *et al.* in [28] fulfills these conditions and at the same time has the advantage of simplicity that makes it suitable for extensive phenomenological studies. We will use this form of EOS for color superconducting quark matter phases that was reused in several studies and in Ref. [29] given the form

$$P = \frac{\xi_4 a_4}{4\pi^2} \mu^4 + \frac{\xi_{2a} \Delta^2 - \xi_{2b} m_s^2}{\pi^2} \mu^2 - B_{\text{eff}}, \quad (1)$$

where the quark chemical potential μ is equivalently expressed through the baryon one $\mu_B = 3\mu$ and for the color-flavor-locking (CFL) phase holds that $\xi_4 = 3$, $\xi_{2a} = 3$ and $\xi_{2b} = 3/4$. This model has the disadvantage that it uses four free parameters for which rather wide margins exist: (1) the coefficient $a_4 = 1 - 2\alpha_s/\pi$ that depends on the running fine structure constant of the strong interaction α_s in first order; (2) the diquark pairing gap Δ ; (3) the effective bag pressure B_{eff} ; and (4) the strange quark mass m_s .

It has, however, the advantage that it is very easy to use and allows to scan the space of opportunities for discussing color superconducting quark matter in NSs, bound to observational constraints for masses and radii. For example, in Ref. [30], this model was employed in order to conclude immediately after the first Shapiro-delay based mass measurement on PSR J1614-2230 [31] (which was revised in [32]) that a lower limit of $1.93 M_\odot$ for maximum mass of NSs would entail that quark matter has to be strongly interacting ($a_4 < 0.63$) and color superconducting ($a_2 = m_s^2 - 4\Delta^2 < m_s^2$) when the onset of deconfinement is set to $1.5 n_0$ by an appropriate choice of B_{eff} .

In this work, we will consider the CFLl phase that allows to neglect the parameter m_s and suggest to fix the remaining three parameters by fitting them to the diquark gap and the pressure of the nonlocal NJL model [33,34]. In the latter, the scalar-pseudoscalar coupling, the light current quark mass and the range of the interaction are determined by low-energy vacuum QCD phenomenology, the pion mass and decay constant as well as the chiral condensate. The remaining unknown coupling constants in the vector meson and diquark interaction channels, G_V and G_D , will be mapped to the parameters of the ABPR model and can be constrained by the NS phenomenology. In this way, the present work will allow to link the parameters of an effective low-energy QCD Lagrangian to the effective ABPR quark matter model that is convenient to use in NS phenomenology and has the attractive feature of an asymptotic approach to the conformal limit which is in accordance with pQCD.

II. COLOR SUPERCONDUCTING QUARK MATTER

A. The ABPR model

In the following we will discuss a CFLl phase, where the strange quark has the same current mass as the up and down quarks, i.e. $m_u = m_d = m_s = m$. For practical purposes $m = 0$ can be used as an excellent approximation. In this phase all quark species are equivalent and subject to the same pairing gap Δ . Then, their distribution functions become degenerate and consequently the partial densities are equal. This entails that the CFLl quark matter is neutral with respect to electric and color charges. Therefore, no

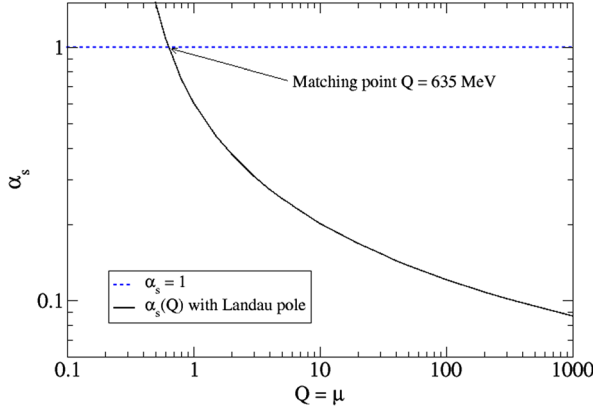


FIG. 1. Running coupling $\alpha_s(Q = \mu)$ according to 1-loop β function (black solid line) with a Landau pole at $Q = \Lambda = 315$ MeV and a constant coupling at the level of the freezing value $\alpha_s(0) \sim 1$ (blue dotted line) which leads to a matching point at $Q = \mu = 635$ MeV.

leptons will appear in CFL matter. For the coefficient $a_4(\mu) = 1 - 2\alpha_s(\mu)/\pi$ we will use two cases that are glued together at a matching point $\mu_{\text{MP}} = 635$ MeV,

$$\alpha_s(\mu) = \begin{cases} 1, & \text{if } \mu < \mu_{\text{MP}} \\ 4\pi/[\beta_0 \ln(\mu^2/\Lambda^2)], & \text{otherwise,} \end{cases} \quad (2)$$

where $\beta_0 = 11 - 2N_f/3$ and $\Lambda = 315$ MeV, see Fig. 1.

The resulting three-flavor, color superconducting quark matter EoS reads

$$P = \frac{3}{4\pi^2} a_4(\mu) \mu^4 + \frac{3}{\pi^2} \Delta^2 \mu^2 - B_{\text{eff}}, \quad (3)$$

where the a_4 coefficient becomes medium dependent for chemical potentials above the matching point $\mu > \mu_{\text{MP}}$ where the strong coupling $\alpha_s(\mu)$ starts to run. For the quark number density follows

$$\begin{aligned} n &= \frac{\partial P}{\partial \mu} \\ &= \frac{3}{\pi^2} \left(a_4 + \frac{a'_4}{4} \mu \right) \mu^3 + \frac{6}{\pi^2} \Delta^2 \mu, \end{aligned} \quad (4)$$

and the energy density is thus

$$\begin{aligned} \varepsilon &= \mu n - P \\ &= \frac{9}{4\pi^2} \left(a_4 + \frac{a'_4}{3} \mu \right) \mu^4 + \frac{3}{\pi^2} \Delta^2 \mu^2 + B_{\text{eff}}. \end{aligned} \quad (5)$$

An interesting quantity is the squared sound speed which serves as a measure for the stiffness of the EOS. It is obtained as

$$\begin{aligned} c_s^2 &= \frac{dP}{d\varepsilon} = \frac{n d\mu}{\mu dn} \\ &= \frac{1 + \zeta}{3 + \zeta} \left[1 - \frac{a'_4}{3} \mu \right] + \mathcal{O}(\alpha_s^3), \end{aligned} \quad (6)$$

where we introduced μ -dependent function

$$\zeta = \frac{18\Delta^2}{\mu_B^2} \left[a_4 + \frac{a'_4}{4} \mu \right]^{-1}. \quad (7)$$

In our simple model (2) for the running coupling, we obtain for the μ -derivative of the coefficient a_4

$$a'_4 = \frac{d}{d\mu} \left(1 - \frac{2\alpha_s}{\pi} \right) = \begin{cases} 0, & \text{if } \mu < \mu_{\text{MP}} \\ \frac{\beta_0}{\pi^2} \alpha_s^2 \frac{1}{\mu}, & \text{otherwise.} \end{cases} \quad (8)$$

We would like to discuss the two limiting cases of the matching model for a running $\alpha_s(\mu)$ shown in Fig. 1.

In the first case ($\alpha_s = \text{const}$) and for normal quark matter, when $\Delta = 0$, the squared sound speed obeys the “conformal limit” value $c_s^2 = 1/3$. Immediately after the deconfinement transition, when $\mu_B \approx \mu_c \approx 1150$ MeV and for large diquark pairing gap, $\Delta \approx 150$ MeV, the parameter $\zeta(\mu_c) \approx 1$ may be attained for $a_4 = 0.3$ so that $c_s^2(\mu_c) = 1/2$. This value has been obtained as a typical result for several parametrizations of a nonlocal chiral quark model [34,35]. The behavior of the squared sound speed in this case is shown in Fig. 2.

In the second case and for normal matter, $\zeta = 0$, the squared sound speed approaches the “conformal limit” value $c_s^2 = 1/3$ from below for large μ . When in this case we consider a nonvanishing diquark gap, the squared sound speed has a profile similar to the one of the quarkyonic matter, rising to a peak above the conformal limit which is followed by a dip and asymptotically, for large μ , approaching $c_s^2 = 1/3$ from below.

B. Nonlocal NJL model for the CFL phase

A simplified description of color superconducting three flavor quark matter assumes the same current mass m of all quark flavors. Consequently, in such a model all quark flavors are degenerate and have the same partial densities. This entails color and electric charge neutrality of this quark matter as well as a flavor independent quark chemical potential $\mu = \mu_B/3$. In the case of the CFL phase, the microscopic states of paired quarks split into singlet and octet ones. The singlet states are characterized by the pairing gap of amplitude 2Δ , being twice the one of the octet states for which the pairing gap amplitude is Δ . Below we label these states with the subscript index $j = \text{sing}$ for singlets and $j = \text{oct}$ for octets. The assumption about the degeneration of the quark flavor states determines the CFL phase. In this work we model such phase of quark matter with a version of the nonlocal NJL model in the spirit of Ref. [34].

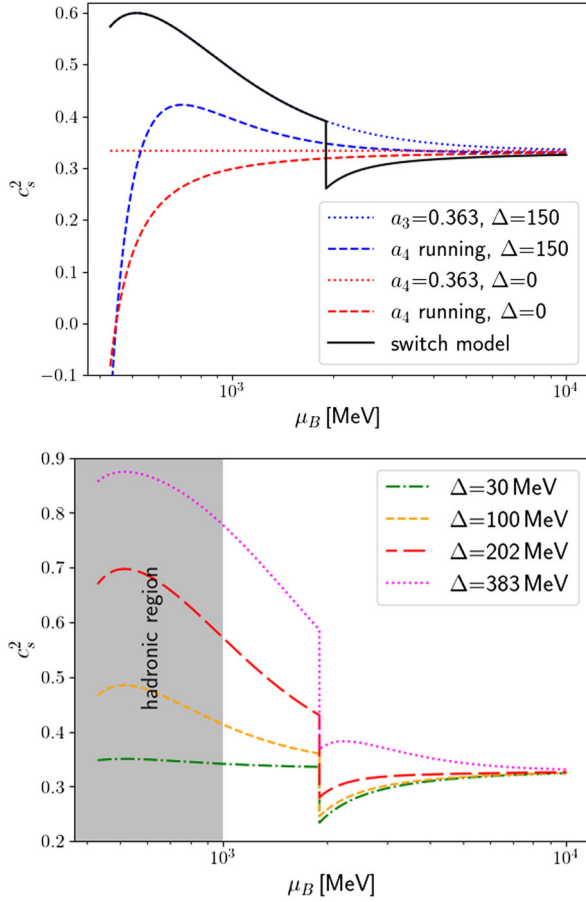


FIG. 2. Upper panel: c_s^2 vs μ_B for constant $a_4 = 0.363$ and for running coupling, as well as for diquark gap $\Delta = 150$ MeV and $\Delta = 0$. The solid black line corresponds to the instant switch model for α_s with a matching point at $\mu_B = 1905$ MeV, see Fig. 1. Lower panel: c_s^2 vs μ_B in the instant switch model for α_s for $a_4 = 0.363$ and four cases of a constant diquark gap $\Delta = 30, 100, 202,$ and 383 MeV.

Within this approach different interaction channels appear as correlations of quark currents, which are propagated through space via the three-momentum dependent form-factor $g_{\mathbf{k}}$. In this work we adopt the Gaussian parametrization of $g_{\mathbf{k}} = \exp(-\mathbf{k}^2/\Lambda^2)$ where Λ determines the finite range of the interaction in momentum space and replaces the constant cutoff parameter of the local NJL model. We follow Ref. [34] and set $\Lambda = 885.47$ MeV. The chiral dynamics of the present model is represented by the melting of the mass gap amplitude σ from some large vacuum value σ_0 . In what follows the subscript index “0” labels the quantities defined in the vacuum, i.e. at $\mu_B = 0$. The mass gap amplitude enters the momentum dependent effective quark mass as $M_{\mathbf{k}} = m + \sigma_{\mathbf{k}}$ with $\sigma_{\mathbf{k}} \equiv \sigma g_{\mathbf{k}}$. We adopt the current quark mass $m = 2.29$ MeV from Ref. [34]. Effects of the vector repulsion are controlled by the zeroth component of the vector meson field (see Refs. [16,34] for details), i.e. by ω . Similar to Ref. [34], we assume the corresponding vector

interaction channel to be local, which formally corresponds to the form-factor $g_{\mathbf{k}}^V = 1$. This simplification allows us to avoid serious technical complications in evaluating the Matsubara sums that would be caused by the appearance of the Matsubara index in the expression for the effective chemical potential of quarks.

With the above notations, the zero temperature thermodynamic potential of the CFL phase can be written as

$$\Omega = \frac{\sigma^2}{4G_S} - \frac{\omega^2}{4G_V} + \frac{\Delta^2}{4G_D} + \Omega_q. \quad (9)$$

Here G_S , G_V , and G_D stand for couplings in the scalar-pseudoscalar, vector, and diquark channels, respectively, and Ω_q is the quark contribution to the thermodynamic potential. Two of the above couplings are parametrized by the dimensionless quantities $\eta_V \equiv G_V/G_S$ and $\eta_D \equiv G_D/G_S$. Parametrizations of the CFL EOS considered below are labeled with pairs of numbers (η_V, η_D) . For example, (1.3, 0.6) corresponds to an EOS obtained for $G_V = 1.3G_S$ and $G_D = 0.6G_S$. The quark term in Ω is

$$\Omega_q = - \sum_{j,a=\pm} d_j \int \frac{d\mathbf{k}}{(2\pi)^3} \left[\frac{\epsilon_{j\mathbf{k}}^a}{2} - \epsilon_{j\mathbf{k}}^a f_{j\mathbf{k}}^a \right]. \quad (10)$$

The summation in this expression is performed over singlet and octet quark ($a = +$) and antiquark ($a = -$) states. The degeneracy factors of the singlet and octet states are expressed through the spin-flavor-color degeneracy one $d = 2 \times 3 \times 3$ as $d_{\text{sing}} = d/9$ and $d_{\text{oct}} = 8d/9$. The corresponding single particle distribution function $f_{j\mathbf{k}}^a = \theta(-\epsilon_{j\mathbf{k}}^a)$ is given in terms of the single particle energy $\epsilon_{j\mathbf{k}}^a$ shifted by the effective chemical potential $\mu^\pm = \pm\mu \mp \omega$. For definiteness we consider positive baryonic chemical potentials leading to $\mu^+ > 0$ and $\mu^- < 0$. Thus

$$\epsilon_{j\mathbf{k}}^a = \text{sgn}(\epsilon_{\mathbf{k}} - \mu^a) \sqrt{(\epsilon_{\mathbf{k}} - \mu^a)^2 + \Delta_{j\mathbf{k}}^2}, \quad (11)$$

where $\epsilon_{\mathbf{k}} = \sqrt{\mathbf{k}^2 + M_{\mathbf{k}}^2}$ is the single particle energy of unpaired quarks, while $\Delta_{j\mathbf{k}} = \zeta_j \Delta g_{\mathbf{k}}$ with $\zeta_{\text{sing}} = 2$ and $\zeta_{\text{oct}} = 1$ is introduced in order to unify the notations. At $\epsilon_{\mathbf{k}} = \mu^+$, which defines the Fermi momentum k_F , $\epsilon_{j\mathbf{k}}^+$ experiences a discontinuous jump of the amplitude $2\Delta_{j\mathbf{k}}|_{|\mathbf{k}|=k_F}$, which is twice the gap of the energy spectrum of the corresponding quark state. In order to quantify it we introduce the effective pairing gap

$$\Delta_{\text{eff}} \equiv \Delta g_{\mathbf{k}}|_{|\mathbf{k}|=k_F}. \quad (12)$$

The first term in the square brackets in Eq. (10) corresponds to the divergent zero point contribution to the thermodynamic potential. It can be regularized by subtracting the constant vacuum value of Ω . This leads to the regularized thermodynamic potential

$$\Omega_{\text{reg}} = \Omega - \Omega_0. \quad (13)$$

The physical values of the mass gap and pairing gap amplitudes as well as the zeroth component of the vector field can be found by minimizing the regularized thermodynamic potential with respect to σ , ω , and Δ . This yields

$$\sigma = 2G_S \sum_{j,a=\pm} d_j \int \frac{d\mathbf{k}}{(2\pi)^3} \left(\frac{1}{2} - f_{j\mathbf{k}}^a \right) \frac{\epsilon_{\mathbf{k}} - \mu^a}{\epsilon_{j\mathbf{k}}^a} \frac{M_{\mathbf{k}} g_{\mathbf{k}}}{\epsilon_{\mathbf{k}}}, \quad (14)$$

$$\omega = 2G_V \sum_{j,a=\pm} d_j \int \frac{d\mathbf{k}}{(2\pi)^3} \left(\frac{1}{2} - f_{j\mathbf{k}}^a \right) a \frac{\epsilon_{\mathbf{k}} - \mu^a}{\epsilon_{j\mathbf{k}}^a}, \quad (15)$$

$$\Delta = 2G_D \sum_{j,a=\pm} d_j \int \frac{d\mathbf{k}}{(2\pi)^3} \left(\frac{1}{2} - f_{j\mathbf{k}}^a \right) \frac{\Delta}{\epsilon_{j\mathbf{k}}^a} \zeta_j^2 g_{\mathbf{k}}^2. \quad (16)$$

The equations for the amplitudes of the mass and pairing gaps include the zero point terms, which are regular due to the presence of the form-factor under the corresponding momentum integrals. It is also worth mentioning that contrary to the case of local current interaction (see, e.g., Refs. [16,36]), Eqs. (14) and (15) do not include the terms with the Dirac delta-function $\delta(\epsilon_{\mathbf{k}} - \mu^a)$ arising from differentiating $\text{sgn}(\epsilon_{\mathbf{k}} - \mu^a)$ in the dispersion relation (11). This is due to $f_{j\mathbf{k}}^a = 1/2$ at vanishing $\epsilon_{j\mathbf{k}}^a = 0$ providing zero value of the factor $1/2 - f_{j\mathbf{k}}^a$ under the momentum integrals. Having Eqs. (14)–(16) solved we can construct EOS of the CFL phase by defining its pressure $P = -\Omega_{\text{reg}} - \Delta B$, baryon density $n_B = dP/d\mu_B = \omega/6G_V$, energy density $\varepsilon = \mu_B n_B - P$ and squared speed of sound $c_S^2 = dP/d\varepsilon$. The contribution $-\Delta B$ to P is a phenomenological constant pressure shift that could be motivated by a medium dependence in the nonperturbative gluon background (confinement) that is not captured by the nNJL model for the quark dynamics. Such a constant has been introduced, e.g., in Refs. [37–39] in order to regulate the onset density of quark deconfinement.

Before going further we would like to consider the question about the instability of the vacuum with respect to formation of the color superconducting state. This happens if the diquark coupling exceeds some critical value G_D^* . At $G_D = G_D^*$ the second order phase transition to the CFL phase occurs in the vacuum. In other words, $\partial^2 \Omega / \partial \Delta^2 = 0$ at $\Delta = 0$ in the vacuum ($f_{j\mathbf{k}}^a = 0$). This allows us to find the critical value of the diquark coupling as

$$G_D^* = \left[\frac{8d}{3} \int \frac{d\mathbf{k}}{(2\pi)^3} \frac{g_{\mathbf{k}}^2}{\epsilon_{\mathbf{k}}} \right]^{-1} \quad (17)$$

parametrized via $\eta_D^* \equiv G_D^*/G_S$. This expression includes the vacuum value of the mass gap amplitude σ_0 defined by Eq. (14) under the conditions $\Delta = 0$ and $\mu^a = 0$. Adjusting the scalar coupling $G_S = 3.307 \text{ GeV}^{-2}$ so that

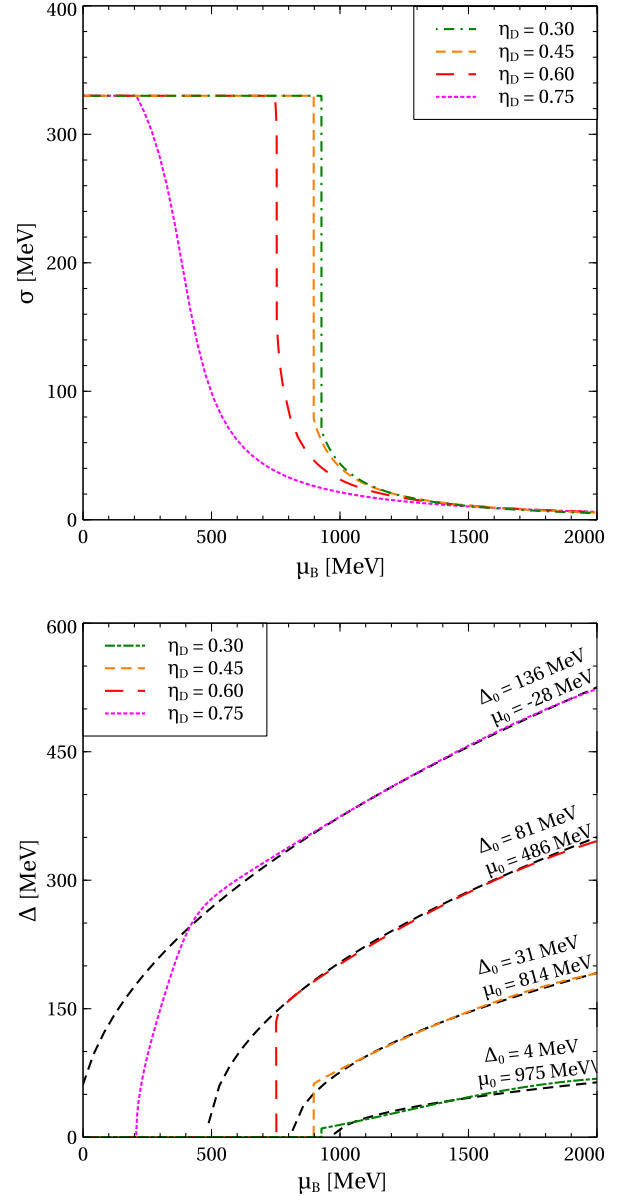


FIG. 3. Amplitude of the mass gap σ (upper panel) and diquark gap Δ (lower panel) as functions of baryonic chemical potential μ_B calculated for vanishing vector coupling $\eta_V = 0$ and diquark couplings η_D given in the legends and $\Delta B = 0$. The black dashed curves on the lower panel represent the results of fitting the pairing gap amplitude by $\Delta = \sqrt{\Delta_0(\mu_B - \mu_0)}$ as discussed in the text.

$\sigma_0 = 330 \text{ MeV}$, we obtain $\eta_D^* = 0.761$. In order to provide vacuum stability we limit our analysis to the values of the diquark coupling respecting the requirement $\eta_D \leq 0.75$.

The amplitudes of the pairing gap Δ and the mass gap σ as functions of the baryonic chemical potential are shown in Fig. 3 for different choices of the diquark coupling η_D . At small but finite value of the baryon chemical potential σ has its vacuum value and Δ vanishes. This corresponds to the chirally broken normal phase of heavy unpaired quarks.

At a certain value of μ_B the mass gap amplitude starts to melt, while the pairing gap amplitude starts to grow. At small $\eta_D \ll 1$ this happens discontinuously, with a jump in the chiral (σ) and color superconductivity (Δ) order parameters, signalling a first order phase transition to the CFL quark matter. At large $\eta_D \simeq 1$, however, this transition is of the second order for the diquark condensate, with the onset starting from $\Delta = 0$ followed by a continuous increase that goes over to a square root behavior

$$\Delta = \sqrt{\Delta_0(\mu_B - \mu_0)} \quad (18)$$

with Δ_0 and μ_0 being constant parameters. For a given value of the diquark coupling these parameters are defined by fitting the pairing gap amplitude within the range of the baryon chemical potentials from $\mu_1 = 1$ GeV to $\mu_2 = 2$ GeV, which covers the values typical for quark matter in NSs. On the lower panel of Fig. 3, we demonstrate the quality of the fit (18) and provide the parameters Δ_0 and μ_0 for four cases of diquark couplings η_D .

Above the color superconductivity onset this square root dependence perfectly describes behavior of Δ . It is interesting to note that this scaling law for the diquark condensate was found in a recent study of lattice simulations of two-color QCD [40].

While Δ grows with μ_B , the momentum form-factor g_k defined at $|\mathbf{k}| = k_F$ exhibits the opposite behavior. As a result the effective pairing gap Δ_{eff} significantly flattens. Its behavior is shown in Fig. 4. Within the range of baryon

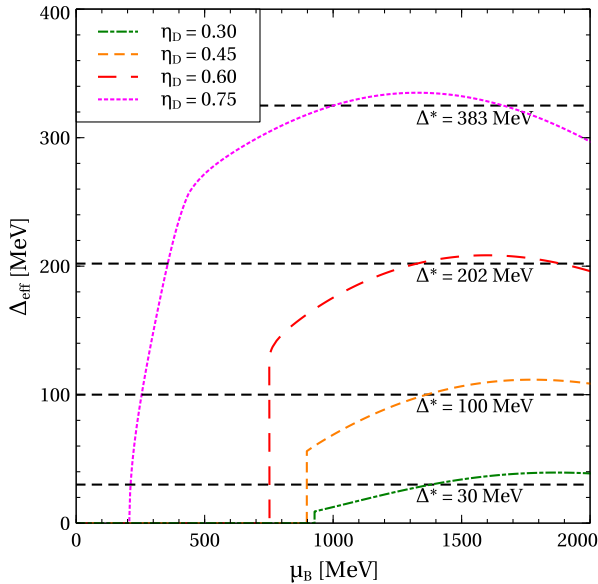


FIG. 4. Effective pairing gap Δ_{eff} as a function of baryonic chemical potential μ_B calculated for vanishing vector coupling $\eta_V = 0$ and diquark couplings η_D given in the legend. The black dashed lines represent the average values of the effective pairing gap Δ^* discussed in the text.

chemical potentials from μ_1 to μ_2 , the effective pairing gap can be approximated by its average value

$$\Delta^* = \frac{1}{\mu_2 - \mu_1} \int_{\mu_1}^{\mu_2} d\mu_B \Delta_{\text{eff}}(\mu_B). \quad (19)$$

It is worth mentioning that this average value is almost insensitive to the vector coupling, which does not impact Δ_{eff} but simply renormalizes μ_B . Larger diquark couplings lead to stronger quark pairing and, consequently, to larger average values of the effective pairing gap of the CFL matter.

For the functional dependence of Δ^* on η_D , we found a quadratic fit, see the upper panel of Fig. 5,

$$\Delta^* [\text{MeV}] = 77.65 - 521 \eta_D + 1233.3 \eta_D^2. \quad (20)$$

On the other hand, η_V regulates the stiffness of the CFL EOS being in one-to-one correspondence with the slope of pressure defined as a function of μ_B . As is seen from Fig. 6, within the range of the baryonic chemical potentials typical for quark matter in the cores of NS the vector coupling can be adjusted so that the pressure slopes of the CFL quark matter and ABPR model coincide. We would like to stress, the stronger is the diquark pairing the weaker should be the

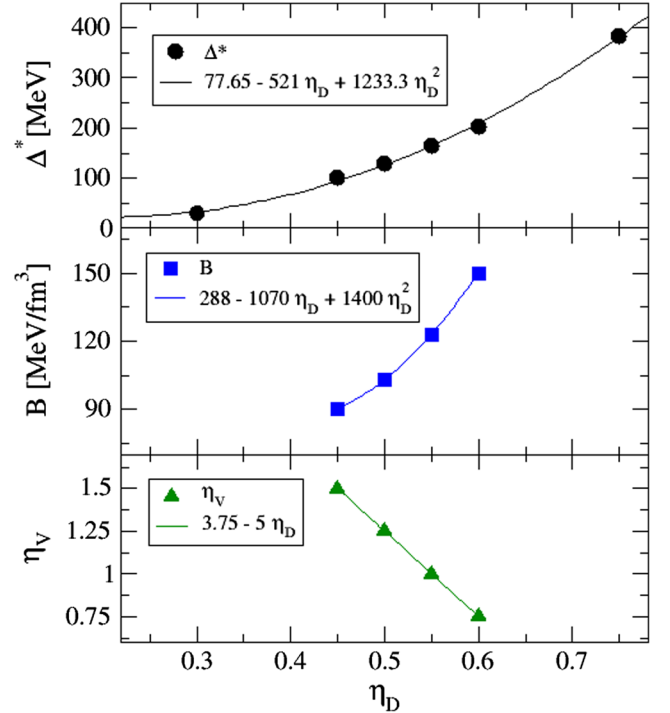


FIG. 5. Dependence of the effective constant diquark gap Δ^* (top panel) and the bag pressure B (middle panel) of the ABPR model on the diquark coupling η_D in the n1NJL model Lagrangian. The bottom panel shows the vector meson coupling η_V required for the matching between n1NJL and ABPR model in the low-energy domain of NS chemical potentials.

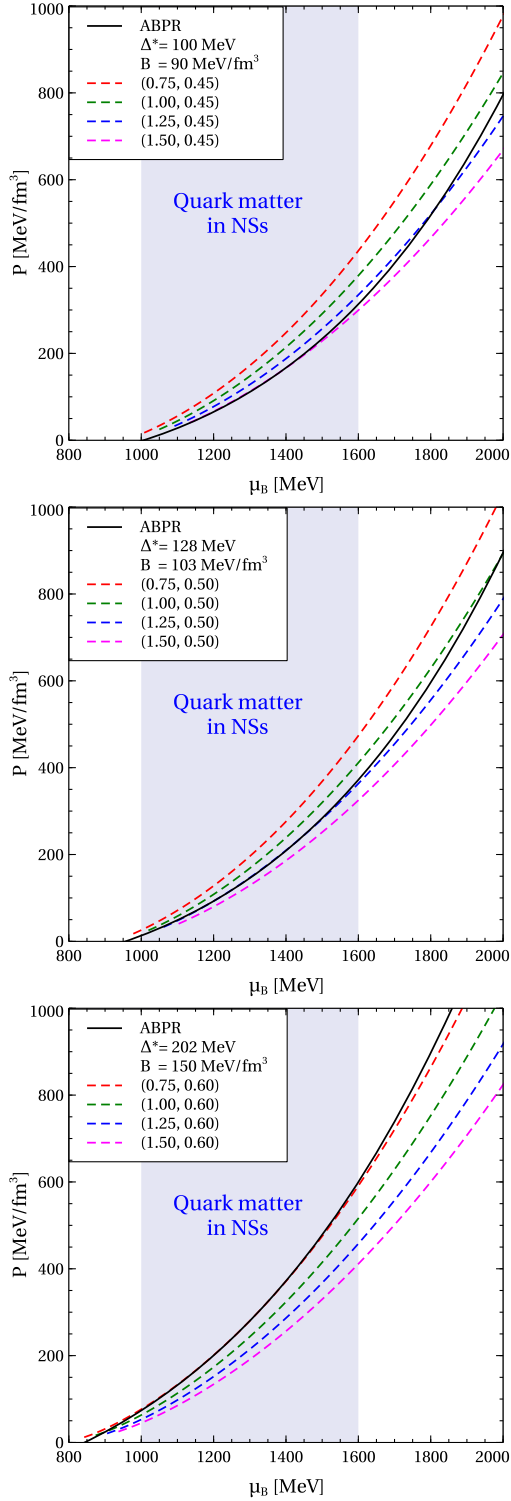


FIG. 6. Pressure of the CFL quark matter P as function of baryonic chemical potential μ_B calculated for several values of η_V indicated in the legends and $\eta_D = 0.45$ (top panel), $\eta_D = 0.5$ (middle panel), and $\eta_D = 0.60$ (bottom panel). The results are compared to the pressure of the ABPR model with the pairing gap Δ^* and bag pressure B_{eff} , which coincides with B for $\Delta B = 0$ shown here. The shaded area represents the approximate range of μ_B typical for quark matter in NSs.

vector repulsion providing the same slopes of the CFL and ABPR pressures. Coincidence of the absolute values of pressures of these two models requires an adjustment of the bag pressure B of the ABPR model, which grows with the diquark coupling, see the lower panel of Fig. 5. Also for this behavior a quadratic fit is found

$$B[\text{MeV}/\text{fm}^3] = 288 - 1070\eta_D + 1400\eta_D^2. \quad (21)$$

To summarize, we note that for a fixed choice of the QCD structure constant α_s , the parametrization of the ABPR model that would provide a matching with the nNJL model describing the CFL quark matter is determined by the choice of the diquark coupling η_D . There is a one-to-one correspondence of this parameter to the constant pairing gap Δ^* expressed by Eq. (20). With a proper choice of η_V that reproduces the curvature of the ABPR pressure in the NS density range, the constant shift B follows unambiguously. There is a linear relationship between η_V and η_D

$$\eta_V = 3.75 - 5.0\eta_D. \quad (22)$$

The complete dictionary can be read-off Fig. 5. This motivates us to establish a connection between relatively simple phenomenological ABPR EOS and microscopic nNJL approach to the CFL quark matter.

C. Parameter matching between ABPR and nNJL models

The ABPR model [28] is built on top of the bag model with pQCD corrections by taking into account the effects of quark pairing in a perturbative manner. The corresponding pressure reads

$$P_{\text{ABPR}} = P_{\text{free}} + P_{\text{pert}} + P_{\text{pair}} - B_{\text{eff}}. \quad (23)$$

The effective bag pressure $B_{\text{eff}} = B + \Delta B$, which is present in Eqs. (1) and (3) absorbs the two constant parameters B and ΔB . It is worth mentioning that B provides consistency of the ABPR and nNJL EOSs, while ΔB is introduced to adjust the onset density of quark deconfinement.

The negative of the regularized thermodynamic potential (13) with $m = \sigma = \omega = \Delta = 0$ yields the pressure of free massless quarks with the single particle energies shifted by the chemical potential $\epsilon_{\mathbf{k}} = |\mathbf{k}| - \mu$ and the distribution function being $\tilde{f}_{\mathbf{k}} = \theta(-\epsilon_{\mathbf{k}})$. Thus

$$P_{\text{free}} = -d \int \frac{d\mathbf{k}}{(2\pi)^3} \epsilon_{\mathbf{k}} \tilde{f}_{\mathbf{k}} = \frac{3}{4\pi^2} \mu^4. \quad (24)$$

The order $\mathcal{O}(\alpha_s)$ perturbative correction P_{pert} can be obtained as a two-loop exchange energy of massless quarks [41]. For $N_f = 3$ flavors and $N_c = 3$ colors it is

$$P_{\text{pert}} = -\frac{N_f(N_c^2 - 1)g^2}{4} \left[\int \frac{d\mathbf{k}}{(2\pi)^3} \frac{\mathbf{f}_{\mathbf{k}}}{\mathbf{e}_{\mathbf{k}}} \right]^2 = -\frac{3\alpha_s}{2\pi^3} \mu^4. \quad (25)$$

Here the QCD structure constant $\alpha_s = g^2/4\pi$ is expressed through the QCD coupling g . The effects of quark pairing can be taken into account by introducing P_{pair} being the negative of Ω_{reg} with $m = \sigma = \omega = 0$ and subtracted P_{free} , i.e.

$$P_{\text{pair}} = \sum_j d_j \int \frac{d\mathbf{k}}{(2\pi)^3} \sqrt{\mathbf{e}_{\mathbf{k}}^2 + \Delta_{j\mathbf{k}}^2} \mathbf{f}_{\mathbf{k}} - P_{\text{free}}. \quad (26)$$

Note, the term $-\Delta^2/4G_D$ [see Eq. (9)] is neglected in this expression since it is small compared to the final result $P_{\text{pair}} \propto \mu^2 \Delta^2$. Naive perturbative treatment of the pairing effects assumes expanding Eq. (26) in powers of the pairing gap amplitude. However, in the present case this procedure is ill defined since already in the leading order correction expansion coefficient diverges logarithmically due to the presence of the factor $-\mathbf{e}_{\mathbf{k}}^{-1}$ under the momentum integral. This requires another expansion parameter, which is proportional to the pairing gap and provides convergence of the expansion coefficients. In order to define such parameter we notice that the main contribution to the momentum integral in Eq. (26) is due to the momenta close by the absolute value to μ . In this case $\mathbf{e}_{\mathbf{k}}$ is small and $\mathbf{e}_{\mathbf{k}} \Delta_{j\mathbf{k}}$ can be used as a proper expansion parameter. In order to make the next step we notice that in the leading order

$$\begin{aligned} \sqrt{\mathbf{e}_{\mathbf{k}}^2 + \Delta_{j\mathbf{k}}^2} &= \sqrt{(\Delta_{j\mathbf{k}} - \mathbf{e}_{\mathbf{k}})^2 + 2\mathbf{e}_{\mathbf{k}} \Delta_{j\mathbf{k}}} \\ &= \Delta_{j\mathbf{k}} - \mathbf{e}_{\mathbf{k}} + \mathcal{O}(\mathbf{e}_{\mathbf{k}} \Delta_{j\mathbf{k}}). \end{aligned} \quad (27)$$

It is important that the leading order correction in this expression includes the factor $\mathbf{e}_{\mathbf{k}}$, which provides convergence of the momentum integrals at the upper limit of integration. Performing some algebra with Eq. (26) and using the above expansion we arrive at

$$\begin{aligned} P_{\text{pair}} &= \sum_j d_j \int \frac{d\mathbf{k}}{(2\pi)^3} \frac{\Delta_{j\mathbf{k}}^2 \mathbf{f}_{\mathbf{k}}}{\sqrt{\mathbf{e}_{\mathbf{k}}^2 + \Delta_{j\mathbf{k}}^2} - \mathbf{e}_{\mathbf{k}}} \\ &= \sum_j d_j \int \frac{d\mathbf{k}}{(2\pi)^3} \frac{\Delta_{j\mathbf{k}}^2 \mathbf{f}_{\mathbf{k}}}{\Delta_{j\mathbf{k}} - 2\mathbf{e}_{\mathbf{k}}} + \mathcal{O}(\Delta^3). \end{aligned} \quad (28)$$

The leading order term in this expression is proportional to the squared pairing gap amplitude as is expected for the ABPR amplitude. At the same time, the order $\mathcal{O}(\Delta^3)$ correction in Eq. (28) is regular due to the presence of the factor $\mathbf{e}_{\mathbf{k}}$ under the momentum integral. As we already mentioned, the main contribution to this integral is due to $|\mathbf{k}| \simeq \mu$. This allows us to replace the factor $\Delta_{j\mathbf{k}}^2$ in Eq. (28) by its value at $|\mathbf{k}| = \mu$, i.e. by $\zeta_j^2 \Delta_{\text{eff}}^2$ since in the considered

case $k_F = \mu$. Due to the same reason we approximate the integration measure as

$$d\mathbf{k} \simeq d(\Delta_{\mathbf{k}} - 2\mathbf{e}_{\mathbf{k}}) \frac{4\pi|\mathbf{k}|^2}{\left. \frac{\partial}{\partial|\mathbf{k}|} (\Delta_{\mathbf{k}} - 2\mathbf{e}_{\mathbf{k}}) \right|_{|\mathbf{k}|=\mu}}. \quad (29)$$

The denominator in this expression is introduced in order to compensate the factor arising from the differential $d(\Delta_{\mathbf{k}} - 2\mathbf{e}_{\mathbf{k}})$. This denominator is $-2 + \mathcal{O}(\Delta)$. With this Eq. (28) gets

$$P_{\text{pair}} = \sum_j \frac{d_j \zeta_j^2 \mu^2 \Delta_{\text{eff}}^2}{(2\pi)^2} \int_0^\mu \frac{d(\Delta_{j\mathbf{k}} - 2\mathbf{e}_{\mathbf{k}})}{\Delta_{j\mathbf{k}} - 2\mathbf{e}_{\mathbf{k}}} + \mathcal{O}(\Delta^3). \quad (30)$$

The momentum integral in Eq. (30) can be carried explicitly. It yields $\ln(2\mu/\zeta_j \Delta_{\text{eff}}) + \mathcal{O}(1)$. Thus, explicitly summing over the singlet and octet states we obtain

$$P_{\text{pair}} = \frac{3}{\pi^2} \mu^2 \Delta_{\text{eff}}^2 \left[\ln \frac{\mu^2}{\Delta_{\text{eff}}^2} + \frac{\ln 2}{6} \right] + \mathcal{O}(\Delta^3). \quad (31)$$

Now we use the limit $\lim_{x \rightarrow 0} x(\ln x^{-1} + c) = x$, which is derived in the Appendix for any constant c , for the case $x = \Delta_{\text{eff}}^2/\mu^2$. It allows us to suppress the square bracket in the previous expression. As it was argued in Sec. II B, in the range of chemical potentials typical for quark matter in NSs the effective pairing gap Δ_{eff} can be substituted by its average value Δ^* . With this the correction caused by quark pairing becomes

$$P_{\text{pair}} = \frac{3}{\pi^2} \mu^2 \Delta^{*2}. \quad (32)$$

Finally, combining Eqs. (23), (24), and (32) we obtain an effective EOS of paired quark matter, which has the well known form of the ABPR model [28]. However, in our formulation the key parameter of this model, i.e. the pairing gap Δ^* , is directly derived from the microscopic nNJL approach and can be straightforwardly connected to the parameters of its Lagrangian.

III. HYBRID EOS AND HYBRID STARS

In order to obtain a hybrid EOS with a (hyper)nuclear hadronic phase at low densities and a transition to the CFL quark matter phase at high densities, we shall employ the two-phase approach. This means that in this work we do not aim at a unified description of quark-hadron matter where the hadronic phase would emerge when starting from a microscopic approach we describe the hadrons as bound states of quarks in going beyond the mean field approximation. Here we restrict ourselves to the latter and chose an appropriate relativistic density functional model to describe the hadronic phase. The transition between both phases is obtained by a Maxwell construction.

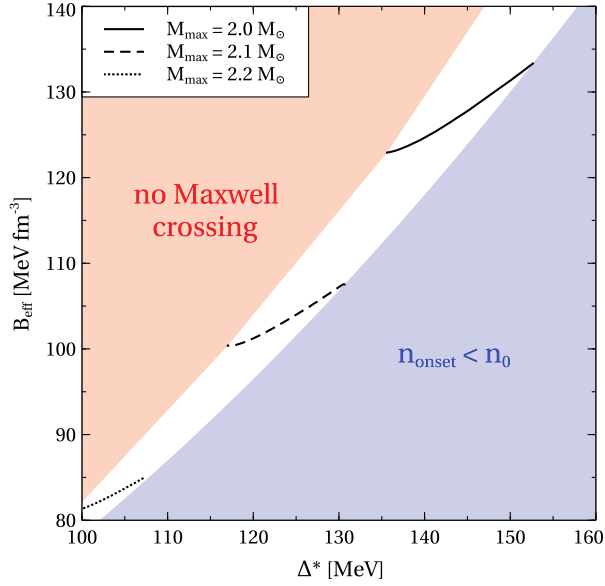


FIG. 7. Admissible free parameters of the ABPR model for a hybrid EOS with DD2npY-T hadronic phase. Between inaccessible regions due to impossibility of a Maxwell construction (red area) and too low onset of deconfinement (blue area), the attainable maximum masses are shown by solid ($2.0M_{\odot}$), dashed ($2.1M_{\odot}$), and dotted ($2.2M_{\odot}$) lines in the white area.

A. Maxwell construction with hadronic EOS

We consider as hadronic EOS the relativistic density functional DD2npY-T with nucleons and hyperons [42], which agrees with the low density constraint from the chiral effective field theory [43].

For the quark matter phase, we employ the ABPR EOS for which we fix the parameter $a_4 = 0.363$ and vary both remaining free parameters, Δ^* and B_{eff} . Performing the Maxwell construction results in a set of hybrid EOS with a first order phase transition that occurs at a critical value of the baryonic chemical potential μ_c and pressure P_c obtained from the Gibbs condition of pressure balance

$$P_c \equiv P_h(\mu_c) = P_q(\mu_c). \quad (33)$$

Note, for a given μ_c hadronic EOS unambiguously defines P_c and critical energy density $\varepsilon_c \equiv \varepsilon_h(\mu_c)$. Since nature prefers the EOS with the higher pressure, the physical pressure at $\mu_B < \mu_c$ is that of the hadronic phase and at $\mu_B > \mu_c$, the hybrid EOS is given by the pressure of the ABPR quark matter model.

In realizing the Maxwell construction, we observe that there is only a small corridor for the free parameters of the ABPR model, see Fig. 7. The strong limitation stems from inaccessible regions in the 2D parameter space due to impossibility of a Maxwell construction (red area) and a too low onset of deconfinement (blue area). In between, there is

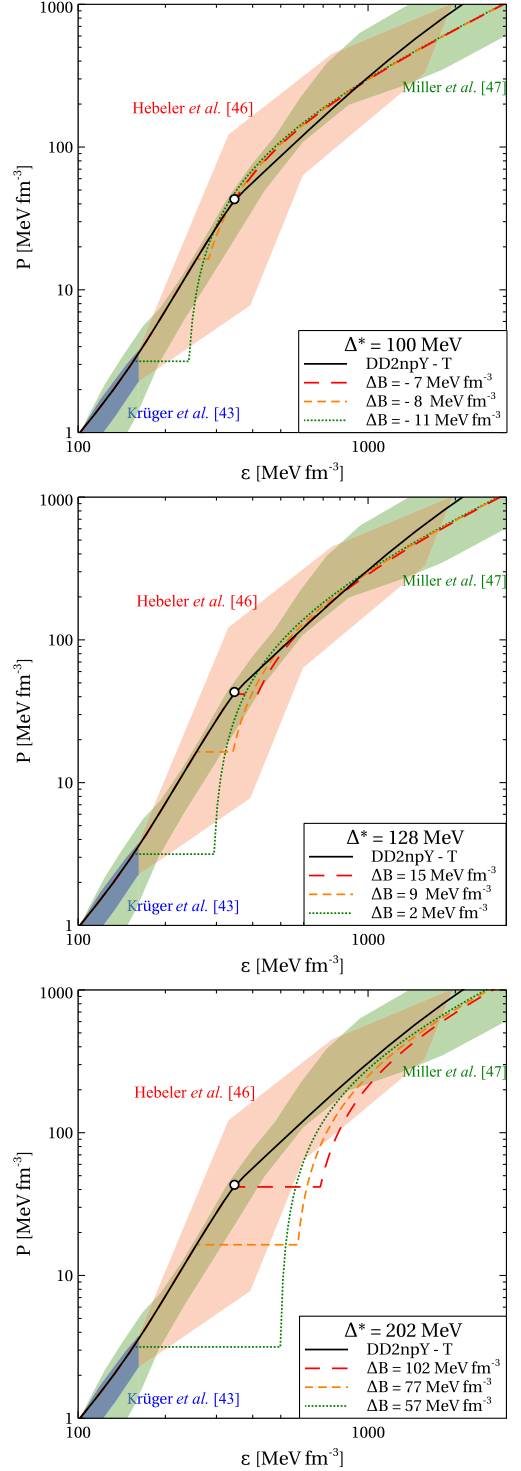


FIG. 8. Pressure P of cold electrically neutral quark-hadron matter in β -equilibrium obtained within the ABPR model with $\Delta^* = 100$ MeV (upper panel), $\Delta^* = 128$ MeV (middle panel), and $\Delta^* = 202$ MeV (lower panel), corresponding to $\eta_D = 0.45$, $\eta_D = 0.5$, and $\eta_D = 0.6$, respectively. An empty circle on the hadronic curves indicates the hyperon onset. The nuclear matter constraints represented by the shaded areas are discussed in the text.

TABLE I. Parameter matching between nNJL model (columns 2 and 3) and the ABPR model (columns 3 and 4) for the chosen case $a_4 = 0.363$. The parameter ΔB is added to both EOS to fix the onset of deconfinement.

Set	η_D	η_V	Δ^* [MeV]	B [MeV/fm ³]	ΔB [MeV/fm ³]	$\Delta\varepsilon$ [MeV/fm ³]	M_{onset} [M_\odot]	M_{max} [M_\odot]	μ_B^{max} [MeV]	ε^{max} MeV/fm ³	$R_{2.0}$ [km]	$R_{1.4}$ [km]	$\Lambda_{1.4}$
I a	0.45	1.5	100	90	-7	0	1.37	2.19	1597	1020	13.05	13.17	678
I b	0.45	1.5	100	90	-8	26	0.84	2.20	1578	1016	12.99	13.04	623
I c	0.45	1.5	100	90	-11	86	0.24	2.23	1570	996	12.85	12.57	565
II a	0.5	1.25	128	103	15	70	1.37	2.03	1617	1217	11.48	13.13	660
II b	0.5	1.25	128	103	9	86	0.84	2.05	1624	1226	11.77	12.32	402
II c	0.5	1.25	128	103	2	139	0.24	2.10	1604	1172	11.74	11.65	349
III a	0.6	0.75	202	150	102	338	1.37	1.64	1740	2014	...	11.10	148
III b	0.6	0.75	202	150	77	316	0.84	1.69	1741	1994	...	9.96	81
III c	0.6	0.75	202	150	57	343	0.24	1.78	1695	1822	...	9.43	88

a white area where hybrid EOS can be found that lead to reasonable hybrid NS sequences.

We note that replacing the Maxwell construction by a crossover interpolation scheme [44] removes the strong constraints on the parameter choice and allows to construct hybrid EOS with color superconductivity that fulfill the observational constraints in a wider parameter range of the ABPR model [45].

Figure 8 shows the hybrid quark-hadron EOSs obtained by matching the DD2npY-T hadronic EOS and the ABPR quark matter ones by means of the Maxwell construction described above. These EOSs agree with the low density constraint from the chiral EFT approach to nuclear matter [43] by construction, and with the multipolytrope analyses of Hebel *et al.* (Ref. [46] with the observational constraint from the high mass of PSR J1614 + 2230) and by Miller *et al.* (Ref. [47] for the combined mass and radius measurement of PSR J0740 + 6620) for the cases of moderate values of diquark gaps $\Delta^* = 100, 128$ MeV. One should bear in mind that the analyses of Refs. [46,47] are not sensitive to the region of central pressures $P(r=0) \lesssim 20$ MeV/fm³, which would correspond to NS masses below $\sim 1.1M_\odot$, where no measurements of pulsar masses and radii exist.¹ For an orientation how to relate a central pressure and mass of hadronic NSs, please regard the open circle on Figs. 8 and 10 that stands for the onset of hyperons in the DD2npY-T EOS.

The Fig. 8 indicates the effect of two parameters of the ABPR EOS, i.e. Δ^* and ΔB . The first of them regulates the jump of the energy density across the hadron-to-quark matter transition $\Delta\varepsilon$. The larger Δ^* the stronger is this jump. At the same time, ΔB controls the onset density n_c of quark deconfinement. Increasing ΔB at a given value of the effective pairing gap Δ^* leads to a larger n_c and smaller $\Delta\varepsilon$.

¹We exclude here the case of the strangely light NS HESS J1731 – 347 [48] which is still under debate, in particular because there is no known mechanism for the formation of such a light compact star with $M = 0.77_{-0.17}^{+0.20}M_\odot$.

In this work we considered only those values of Δ^* and ΔB , which provide positiveness of $\Delta\varepsilon$ across the hadron-to-quark matter transition, being in agreement with the Maxwell construction of a first order phase transition. We list the values of $\Delta\varepsilon$ in Table I.

It is interesting to analyze influence of the effective pairing gap on hybrid EOSs obtained for a given onset density of quark matter. In Fig. 8 such EOSs are depicted by the curves of the same color. As is seen from Fig. 8, increase of Δ^* softens the EOS. At first glance, this conclusion contradicts the increase of the speed of sound for a larger pairing gap (see the lower panel of Fig. 2). In order to resolve this apparent paradox, we consider the dimensionless interaction measure $\delta = 1/3 - P/\varepsilon$. Stiffer EOSs correspond to smaller δ . Inverting $c_s^2 = c_s^2(\mu_B)$, the baryonic chemical potential can be eliminated from the expression for the interaction measure, which can be presented as a function of the speed of sound and bag pressure. A larger c_s^2 leads to smaller values of δ , while increasing B_{eff} causes the opposite effect. Using the Gibbs criterion (33) we express the latter as

$$B_{\text{eff}} = \frac{3}{4\pi^2} a_4 \left(\frac{\mu_c}{3}\right)^4 + \frac{3}{\pi^2} \Delta^{*2} \left(\frac{\mu_c}{3}\right)^2 - P_c. \quad (34)$$

This expression demonstrates that the effective bag pressure grows with Δ^* , as the speed of sound does. As a result, the growth of the pairing gap induces two competing effects: a decrease of δ caused by c_s^2 and its increase due to B_{eff} .

In order to show that within the range of baryonic chemical potentials typical for NSs the second of these effects dominates, we consider the derivative

$$\frac{\partial \delta}{\partial \Delta^*} = \frac{P}{\varepsilon^2} \frac{\partial \varepsilon}{\partial \Delta^*} - \frac{1}{\varepsilon} \frac{\partial P}{\partial \Delta^*}. \quad (35)$$

Using explicit expressions for P , ε , B_{eff} and performing straightforward manipulations, Eq. (35) becomes

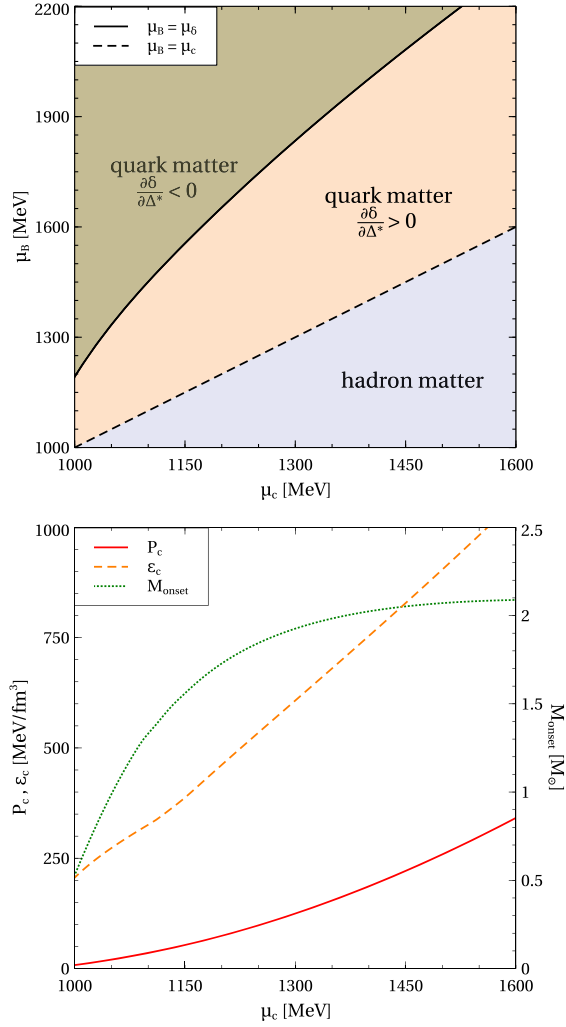


FIG. 9. Ranges of the pairing gap induced softening ($\partial\delta/\partial\Delta^* > 0$) and stiffening ($\partial\delta/\partial\Delta^* < 0$) of the ABPR EOS, separated by μ_δ (upper panel) as well as critical pressure P_c , energy density ϵ_c and onset mass M_{onset} for deconfinement (lower panel) as a function of the critical chemical potential μ_c .

$$\frac{\partial\delta}{\partial\Delta^*} = \frac{12\Delta^*\mu^2}{\pi^2\epsilon^2} \left[P_c - \frac{3a_4}{4\pi^2} \left(\mu^2 - \left(\frac{\mu_c}{3} \right)^2 \right)^2 \right]. \quad (36)$$

From this expression we conclude that δ increases with Δ^* if the baryonic chemical potential is below

$$\mu_\delta = \mu_c \sqrt{1 + 6\pi \sqrt{\frac{3P_c}{a_4\mu_c^4}}}, \quad (37)$$

while at $\mu_B > \mu_\delta$ the interaction measure decreases with the pairing gap growth. This corresponds to the pairing gap induced softening and stiffening of the present EOS, respectively. Since μ_δ always exceeds μ_c , then $\delta > \delta|_{\Delta^*=0}$ after the hadron-to-quark matter phase transition, which corresponds to softening of the ABPR EOS.

The corresponding ranges of the baryonic chemical potential are shown on the upper panel of Fig. 9. On the lower panel of Fig. 9, we show the quantities which characterize the onset of deconfinement, the critical pressure P_c , the critical hadronic energy density ϵ_c . The figure also shows the mass of onset of quark matter in NS M_{onset} , which is discussed below.

B. Calculation of astrophysical observables

There is a one-to-one relationship between an EOS of dense matter and a sequence of NS configurations in the mass-radius diagram which is obtained by solving the Tolman-Oppenheimer-Volkoff (TOV) equations for the spherically symmetric (nonrotating) case [49,50]. These solutions can directly be compared to measurements of mass and radius, e.g., from the combined observations by NICER and XMM Newton of the millisecond pulsar J0740 + 6620 (see the analysis of Miller *et al.* [47]). The mass of this object, $2.08 \pm 0.07 M_\odot$ [51], sets a lower limit for the maximum mass that obtained for a given EOS by solving the TOV equations. Additionally, the tidal deformability of a $1.4 M_\odot$ NSs has been extracted from the gravitational wave measurement of the binary NS merger event GW170818. It has been obtained as $70 < \Lambda < 580$ [52]. The theoretical values of tidal deformability of NSs in dependence of their mass is obtained from solving a system of differential equations with the EOS as an input.

The astrophysical observables were calculated on the basis of the code by Andrea Maselli [53].

C. Observational constraints for EOS parameters

The results for the sequences of star configurations in the mass-radius and tidal deformability-mass diagram are shown in Fig. 10 for three choices of the CFLL diquark pairing gap (upper, middle, and lower panels) with the onset of deconfinement adjusted for each case to $0.24, 0.84$, and $1.37 M_\odot$ by a proper choice of the corrective bag pressure parameter ΔB . The characteristic values for mass, radius and tidal deformabilities are extracted from these solutions and given in Table I. The table also includes values of the baryonic chemical potential μ_B^{max} and energy densities ϵ^{max} reached in the centers of the heaviest NSs with quark cores. Larger diquark couplings or, equivalently, larger constant pairing gaps correspond to softer EOS of quark matter, which leads to larger values of μ_B^{max} and ϵ^{max} . At the same time, for given values of η_D and Δ^* these central chemical potentials and energy densities depend only weakly on the onset mass M_{onset} for quark deconfinement, demonstrating a slightly rising behavior.

Table I indicates that an increase of Δ^* leads to a smaller maximum mass of the NS, which can be interpreted as an apparent softening of the ABPR EOS considered above. Concerning the maximum NS mass it is appropriate to mention that M_{max} is extracted from the solution of the

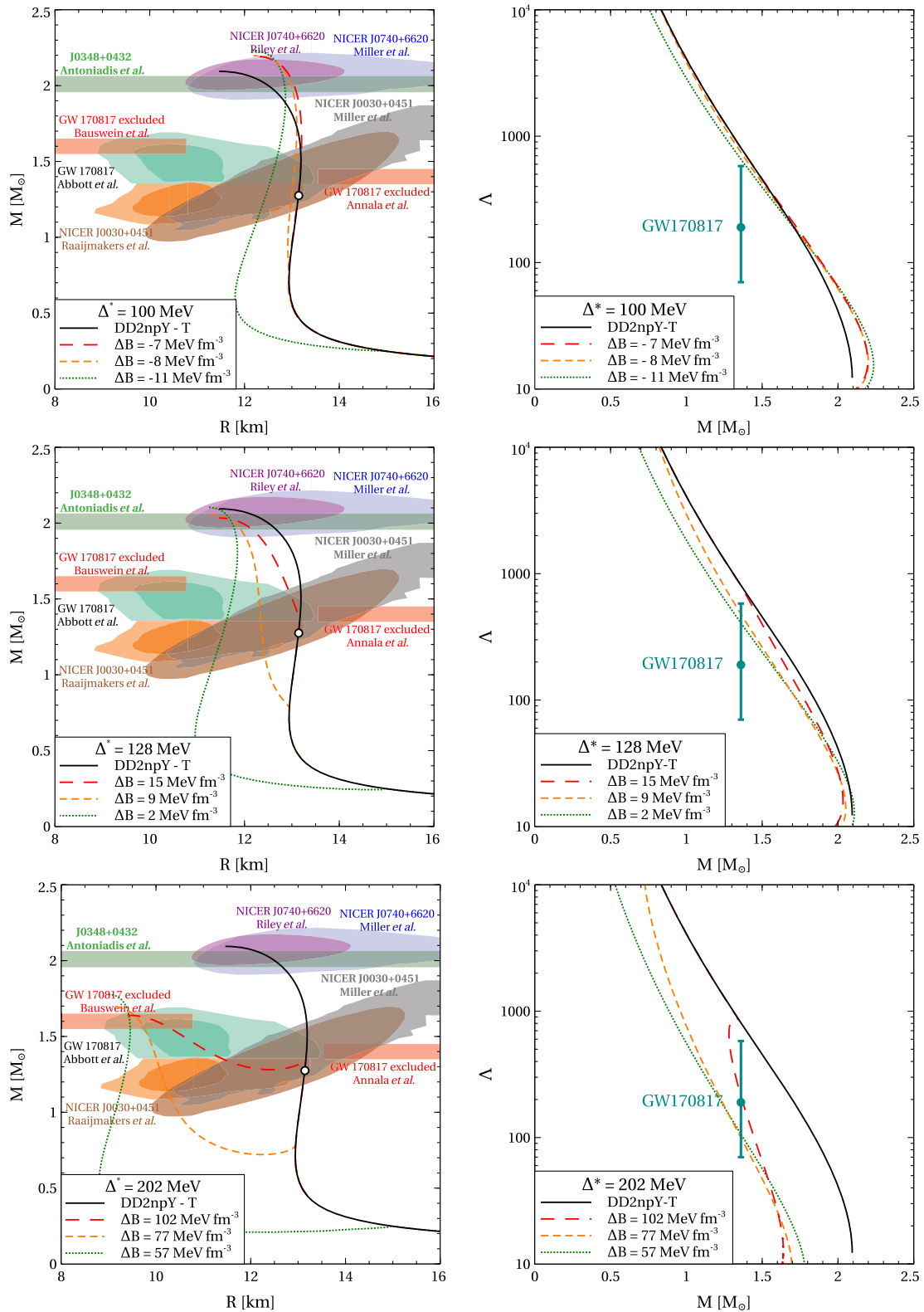


FIG. 10. Left column: Mass-radius relation of hybrid NSs with the quark-hadron EOS presented in Fig. 8. An empty circle on the hadronic curves indicates the hyperon onset. The astrophysical constraints depicted by the colored bands and shaded areas are discussed in the text. Right column: Dimensionless tidal deformability Λ as a function of the NS mass M (upper panel) obtained with the same hybrid EOS that were used in order to obtain the mass-radius relations shown in the left column. The observational constraint on the dimensionless tidal deformability of a $1.4M_{\odot}$ NS is from the binary NS merger GW170817 [52].

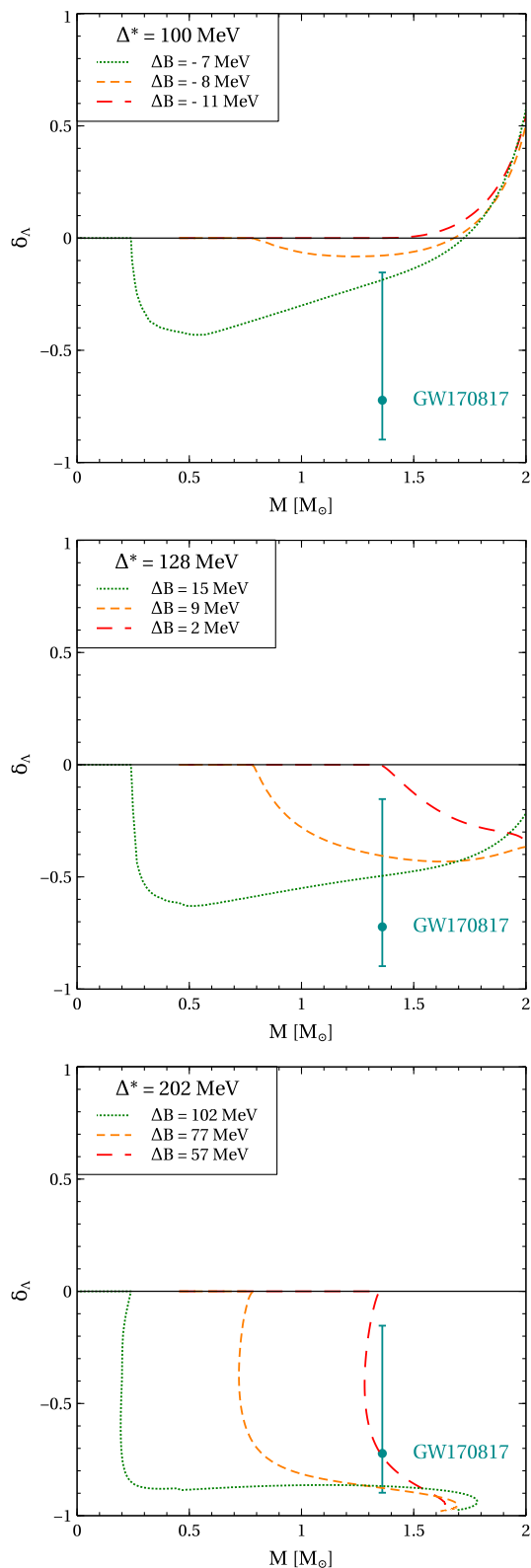


FIG. 11. Relative modification of tidal deformability δ_Λ as a function of the NS mass M calculated with the quark-hadron EOS presented in Fig. 8. The observational constraint from the GW170817 event represented by δ_{GW170817} is discussed in the text.

TOV equation, which does not contain the speed of sound but pressure and energy density. Therefore, within the TOV equation context it is reasonable to quantify the stiffness of an EOS not by the speed of sound but by the dimensionless interaction measure. The analysis of δ performed above, indeed, evidences a softening of the ABPR EOS due to increase of the effective pairing gap and consequent decrease of the NS maximum mass.

The discontinuous behavior of the energy density caused by the first order hadron-to-quark matter transition entails a sizeable reduction of the tidal deformability of hybrid NSs with quark core when compared to NSs with purely hadronic interior. This has been discussed already in Ref. [54], see also the comment on it by Ref. [55]. In order to quantify this effect, we introduce $\delta_\Lambda \equiv (\Lambda - \Lambda_{\text{DD2npY}})/\Lambda_{\text{DD2npY}}$ as a parameter for the relative modification of the tidal deformability compared to the case of purely hadronic NSs represented by Λ_{DD2npY} . In Fig. 11 we show δ_Λ as a function of the NS mass for our sets of hybrid EOSs. A reduction (increase) of Λ corresponds to a negative (positive) δ_Λ when compared to purely hadronic NSs. We show in that figure also δ_Λ for the tidal deformability measurement $\Lambda_{\text{GW170817}} = 190^{+390}_{-120}$ that was extracted from the gravitational wave signal of the binary NS merger GW170817 [52] at the mass of $1.36M_\odot$ for the symmetric case.

The figure indicates that for an early onset of quark deconfinement at $M_{\text{onset}} < 1.4M_\odot$, the tidal deformability of an intermediate mass hybrid NS with quark core is smaller than that of a purely hadronic NS. Thus, a strong and early hadron-to-quark matter phase transition presents a possible solution of the problem of the relatively low tidal deformability $\Lambda_{\text{GW170817}}$. This constraint could not be met by some otherwise well-constrained hadronic matter EOS as, e.g., DD2npY-T. But when an early deconfinement transition with a large $\Delta\epsilon$ occurs (see Table I), this problem can be solved, as Fig. 11 shows. The possibility that the NSs that merged in GW170817 were already hybrid NSs before the merger event and could possibly have been members of a third family branch of NSs, has been discussed already, e.g., in Refs. [56–58].

As a result of the present work and the dictionary we provided, one can constrain the values of the free parameters in the nLNJL model Lagrangian for dense QCD matter with the help of NS phenomenology. To this end, we also indicated in Fig. 7 the isolines of the achievable maximum mass for an admissible pair of ABPR EOS parameters Δ^* and B_{eff} (white region). The larger the chosen Δ^* , the softer the EOS becomes and the smaller is the achievable maximum mass. For $\Delta^* \gtrsim 150$ MeV, the lower limit of the maximum mass cannot be reached. This is also illustrated in Fig. 10 for the case $\Delta^* = 202$ MeV. From Fig. 5 one reads off that the upper limit for $\Delta^* \lesssim 150$ MeV constrains the dimensionless diquark coupling to $\eta_D \lesssim 0.53$. At the same time, for the dimensionless vector coupling holds $\eta_V \gtrsim 1.2$.

IV. CONCLUSIONS

In this work, we have derived the effective cold quark matter model by Alford, Braby, Paris, and Reddy (ABPR) from a nonlocal Nambu–Jona-Lasinio model for the color superconducting quark matter in the CFL phase with three light flavors.

We have discussed a generalization of the ABPR model that uses an $\mathcal{O}(\alpha_s)$ perturbative QCD correction with a running strong coupling constant $\alpha_s(\mu)$ that assures reaching the conformal limit for the squared speed of sound $c_s^2 - 1/3 \rightarrow 0^-$ for high chemical potentials. Below a matching point that is shown to lie above the range of chemical potentials that can be accessed in NSs, the running coupling is switched to a constant value $\alpha_s = 1$ which is large enough to provide the necessary stiffness of the quark matter phase for reaching maximum masses of hybrid stars in accordance with the observational lower limit $M_{\max} \geq 2.01M_\odot$.

We have shown that due to the momentum dependence of the pairing which is induced by the nonlocality of the interaction, the effective gap parameter in the EOS model has a plateau-like behavior in the range of chemical potentials for NSs that is well approximated by a constant value. The dependence of this value on the diquark coupling strength in the nNJL model Lagrangian could be fitted to a parabola. NS phenomenology constrains this pairing gap parameter to values between 100 and 150 MeV which translate to the narrow range of diquark couplings $\eta_D = 0.45 \dots 0.53$. Due to this large pairing gap, the sound speed of the ABPR EOS exceeds the conformal limit value.

The dictionary for translating the vector meson and diquark coupling as free parameters of the nNJL model to those of the ABPR model that is completed by relating the effective bag pressure parameter to the vector meson coupling. In order to fulfill also the low tidal deformability constraint from GW170817, a softening of the EOS on the hybrid NS branch is necessary which requires an early onset of quark deconfinement at $M_{\text{onset}} < 1.4M_\odot$. In order to illustrate this fact, we have introduced a new parameter, the relative change of the tidal deformability due to the phase transition compared to a hadronic baseline (DD2npY-T) and discussed it for the hybrid NS sequences that resulted from parametrizations of the color superconducting quark matter EOS considered in this work. To assure the early onset, a small pressure correction of $\Delta B \sim 10 \text{ MeV/fm}^3$ is required which could be justified by a modification of the non-perturbative gluon sector at high baryon densities.

Summarizing, we have provided a microphysical justification for the use of the ABPR EOS in NS phenomenology based on the nonlocal NJL model for color superconducting quark matter in the CFL phase. A dictionary is provided for relating the ABPR EOS parameters for which constraints from the analysis of NS phenomenology are fulfilled to the free parameters of the nNJL model Lagrangian for low-energy QCD. We find that a finite

pairing gap corresponds to a squared sound speed that exceeds the conformal limit. Increasing the diquark coupling and thus the pairing gap, however, softens the EOS and entails a lowering of the maximum mass. An optimal diquark pairing gap for which the maximum mass exceeds $2M_\odot$ is of the order of 100...120 MeV.

There are several routes one could follow in subsequent work, based on the present study. In concluding, we would like to mention a few of them. The assumption of the degeneracy of the strange quark mass with that of the up and down quarks could be relaxed. Then, one could follow the route of the nonlocal NJL model for that case, or one could employ the approach of the confining density functional [19] which has been recently developed by two of us (D. B., O. I.). The main difference would be in the phase structure that is to be expected, namely the existence or non-existence of a two-flavor color superconducting (2SC) phase and the possibility to address in a microscopic model the case of absolutely stable strange quark matter. Besides the simple Maxwell construction of a hadron-to-quark matter transition, a crossover transition could be constructed, eventually with a corridor of a first-order transition and two critical endpoints. The appropriate method of a two-zone interpolation scheme [20] has been developed by two of us (O. I., D. B.). Also, the simple ansatz of the switch model for the running coupling could be systematically developed. As a first step, one could choose different values of the saturated (constant) coupling in the nonperturbative domain. This would change the switch point and eventually lead to an intrusion of the region where the coupling is running to the NS density domain. Such a variation of the a_4 parameter of the ABPR model would then be reflected in a variation of the η_V parameter of the nNJL model independently of the η_D parameter. A more realistic ansatz for the running of the QCD coupling in the nonperturbative domain [59] could be chosen. Then, a direct influence of the detailed scheme of such a running coupling like, e.g., that of the analytic perturbation theory, on the NS phenomenology would be expected.

ACKNOWLEDGMENTS

The work of D. B., O. I. and U.S. has been supported in part by the Polish National Science Centre (NCN) under Grant No. 2019/33/B/ST9/03059. U.S. acknowledges a stipend from the International Max Planck Research School for “Many-Particle Systems in Structured Environments” at the Max-Planck Institute for Physics of Complex Systems. S.L. thanks JINR Dubna for hospitality and support during part of this work. The authors acknowledge the COST Action No. CA16214 “PHAROS” for supporting their networking activities, in particular the PHAROS Training School on “Equation of State of Dense Matter and Multi-Messenger Astronomy” in Karpacz, June 13–19, 2021.

APPENDIX: LIMIT OF EQ. (30)

Here for the readers convenience we derive the relation

$$\lim_{x \rightarrow 0} x^a \left(\ln \frac{1}{x} + c \right) = \lim_{x \rightarrow 0} \frac{x^a}{a}. \quad (\text{A1})$$

In Sec. II C it is used at $a = 1$, while for the sake of generality we derive it for any nonvanishing a . At the first step we rewrite $x^a = 1/x^{-a}$. This yields an indeterminate

form $\left(\frac{\infty}{\infty}\right)$. It can be treated using the L'Hôpital's rule assuming replacement of $\ln \frac{1}{x} + c$ and x^{-a} by their derivatives. Thus

$$\lim_{x \rightarrow 0} x^a \left(\ln \frac{1}{x} + c \right) = \lim_{x \rightarrow 0} \left(-\frac{1}{x} \right) / \left(-\frac{a}{x^{a+1}} \right). \quad (\text{A2})$$

After a simple algebra this relation arrives at the desired form of Eq. (A1).

-
- [1] H. A. Bethe, G. E. Brown, and J. Cooperstein, *Nucl. Phys.* **A462**, 791 (1987).
- [2] E. Witten, *Phys. Rev. D* **30**, 272 (1984).
- [3] E. Farhi and R. L. Jaffe, *Phys. Rev. D* **30**, 2379 (1984).
- [4] G. Baym, E. W. Kolb, L. D. McLerran, T. P. Walker, and R. L. Jaffe, *Phys. Lett.* **160B**, 181 (1985).
- [5] C. Alcock, E. Farhi, and A. Olinto, *Astrophys. J.* **310**, 261 (1986).
- [6] C. Alcock, E. Farhi, and A. Olinto, *Phys. Rev. Lett.* **57**, 2088 (1986).
- [7] P. Haensel, J. L. Zdunik, and R. Schaeffer, *Astron. Astrophys.* **160**, 121 (1986).
- [8] G. Baym, *Nucl. Phys.* **A479**, 27c (1988).
- [9] D. Blaschke, T. Tovmasian, and B. Kämpfer, *Sov. J. Nucl. Phys.* **52**, 675 (1990).
- [10] G. Röpke, D. Blaschke, and H. Schulz, *Phys. Rev. D* **34**, 3499 (1986).
- [11] M. A. R. Kaltenborn, N.-U. F. Bastian, and D. B. Blaschke, *Phys. Rev. D* **96**, 056024 (2017).
- [12] U. H. Gerlach, *Phys. Rev.* **172**, 1325 (1968).
- [13] S. Benic, D. Blaschke, D. E. Alvarez-Castillo, T. Fischer, and S. Typel, *Astron. Astrophys.* **577**, A40 (2015).
- [14] S. P. Klevansky, *Rev. Mod. Phys.* **64**, 649 (1992).
- [15] M. Buballa, *Phys. Rep.* **407**, 205 (2005).
- [16] T. Klähn, D. Blaschke, F. Sandin, C. Fuchs, A. Faessler, H. Grigorian, G. Röpke, and J. Trümper, *Phys. Lett. B* **654**, 170 (2007).
- [17] T. Klähn, R. Lastowiecki, and D. B. Blaschke, *Phys. Rev. D* **88**, 085001 (2013).
- [18] G. Baym, T. Hatsuda, T. Kojo, P. D. Powell, Y. Song, and T. Takatsuka, *Rep. Prog. Phys.* **81**, 056902 (2018).
- [19] O. Ivanytskyi and D. Blaschke, *Phys. Rev. D* **105**, 114042 (2022).
- [20] O. Ivanytskyi and D. Blaschke, *Eur. Phys. J. A* **58**, 152 (2022).
- [21] D. Blaschke, O. Ivanytskyi, and M. Shahrabaf, in *New Phenomena and New States of Matter in the Universe. From Quarks to Cosmos*, edited by C. Z. Vasconcellos, P. O. Hess, and T. Boller (World Scientific, Singapore, 2022), pp. 1–27.
- [22] M. Alford and K. Rajagopal, *J. High Energy Phys.* **06** (2002) 031.
- [23] K. Rajagopal and F. Wilczek, *Phys. Rev. Lett.* **86**, 3492 (2001).
- [24] O. Komoltsev and A. Kurkela, *Phys. Rev. Lett.* **128**, 202701 (2022).
- [25] S. Typel *et al.* (CompOSE Core Team), *Eur. Phys. J. A* **58**, 221 (2022).
- [26] O. Ivanytskyi and D. Blaschke, *Particles* **5**, 514 (2022).
- [27] O. Ivanytskyi, D. Blaschke, T. Fischer, and A. Bauswein, *EPJ Web Conf.* **274**, 07010 (2022).
- [28] M. Alford, M. Braby, M. W. Paris, and S. Reddy, *Astrophys. J.* **629**, 969 (2005).
- [29] C. Zhang and R. B. Mann, *Phys. Rev. D* **103**, 063018 (2021).
- [30] F. Özel, D. Psaltis, S. Ransom, P. Demorest, and M. Alford, *Astrophys. J. Lett.* **724**, L199 (2010).
- [31] P. Demorest, T. Pennucci, S. Ransom, M. Roberts, and J. Hessels, *Nature (London)* **467**, 1081 (2010).
- [32] Z. Arzoumanian *et al.* (NANOGrav Collaboration), *Astrophys. J. Suppl. Ser.* **235**, 37 (2018).
- [33] S. M. Schmidt, D. Blaschke, and Y. L. Kalinovsky, *Phys. Rev. C* **50**, 435 (1994).
- [34] G. A. Contrera, D. Blaschke, J. P. Carlomagno, A. G. Grunfeld, and S. Liebing, *Phys. Rev. C* **105**, 045808 (2022).
- [35] S. Antić, M. Shahrabaf, D. Blaschke, and A. G. Grunfeld, *arXiv:2105.00029*.
- [36] D. Blaschke, S. Fredriksson, H. Grigorian, A. M. Öztas, and F. Sandin, *Phys. Rev. D* **72**, 065020 (2005).
- [37] G. Pagliara and J. Schaffner-Bielich, *Phys. Rev. D* **77**, 063004 (2008).
- [38] D. Blaschke, J. Berdermann, and R. Lastowiecki, *Prog. Theor. Phys. Suppl.* **186**, 81 (2010).
- [39] L. Bonanno and A. Sedrakian, *Astron. Astrophys.* **539**, A16 (2012).
- [40] K. Iida, E. Ito, and T.-G. Lee, *J. High Energy Phys.* **01** (2020) 181.
- [41] J. I. Kapusta, *Finite Temperature Field Theory*, Cambridge Monographs on Mathematical Physics (Cambridge University Press, Cambridge, 1989), ISBN 978-0-521-35155-3.
- [42] M. Shahrabaf, D. Blaschke, S. Typel, G. R. Farrar, and D. E. Alvarez-Castillo, *Phys. Rev. D* **105**, 103005 (2022).
- [43] T. Krüger, I. Tews, K. Hebeler, and A. Schwenk, *Phys. Rev. C* **88**, 025802 (2013).

- [44] J. I. Kapusta and T. Welle, *Phys. Rev. C* **104**, L012801 (2021).
- [45] D. Blaschke, E. O. Hanu, and S. Liebing, *Phys. Rev. C* **105**, 035804 (2022).
- [46] K. Hebeler, J. M. Lattimer, C. J. Pethick, and A. Schwenk, *Astrophys. J.* **773**, 11 (2013).
- [47] M. C. Miller *et al.*, *Astrophys. J. Lett.* **918**, L28 (2021).
- [48] V. Doroshenko, V. Suleimanov, G. Pühlhofer, and A. Santangelo, *Nat. Astron.* **6**, 1444 (2022).
- [49] R. C. Tolman, *Phys. Rev.* **55**, 364 (1939).
- [50] J. R. Oppenheimer and G. M. Volkoff, *Phys. Rev.* **55**, 374 (1939).
- [51] E. Fonseca *et al.*, *Astrophys. J. Lett.* **915**, L12 (2021).
- [52] B. P. Abbott *et al.* (LIGO Scientific, Virgo Collaborations), *Phys. Rev. Lett.* **121**, 161101 (2018).
- [53] A. Maselli, <https://andreamaselli85.wixsite.com/home/copy-of-geo>.
- [54] S. Postnikov, M. Prakash, and J. M. Lattimer, *Phys. Rev. D* **82**, 024016 (2010).
- [55] J. Takátsy and P. Kovács, *Phys. Rev. D* **102**, 028501 (2020).
- [56] V. Paschalidis, K. Yagi, D. Alvarez-Castillo, D. B. Blaschke, and A. Sedrakian, *Phys. Rev. D* **97**, 084038 (2018).
- [57] D. Blaschke, A. Ayriyan, D. E. Alvarez-Castillo, and H. Grigorian, *Universe* **6**, 81 (2020).
- [58] A. Bauswein and S. Blacker, *Eur. Phys. J. Special Topics* **229**, 3595 (2020).
- [59] A. Deur, S. J. Brodsky, and G. F. de Teramond, *Nucl. Phys.* **90**, 1 (2016).